Real-Time Evolution of the Distribution of Nanoparticles in an Ultrathin-Polymer-Film-Based Waveguide

Suresh Narayanan,[1] Dong Ryeol Lee,[1] Rodney S. Guico,[1,2] Sunil K. Sinha,[3] and Jin Wang[1]
[1]*Advanced Photon Source, Argonne National Laboratory, Argonne, Illinois 60439, USA*
[2]*Department of Materials Science and Engineering, Northwestern University, Evanston, Illinois 60208, USA*
[3]*Department of Physics, University of California, La Jolla, California 92093, USA*
and Los Alamos National Laboratory, Los Alamos, New Mexico 87545, USA
(Received 13 October 2004; published 15 April 2005)

We report a novel application of an ultrathin-polymer-film-based, resonance-enhanced x-ray waveguide as a real-time nanoprobe for elucidating dilute, yet disordered, gold nanoparticles embedded in the polymer matrix. This nanoprobe promises a sensitivity enhancement of several orders of magnitude, hence revealing in real time the lateral nanoparticle distribution with subnanometer spatial resolution. We observed that the motion of the nanoparticles is strongly anisotropic, with in-plane coalescence taking place more rapidly than out-of-plane diffusion, which can ultimately facilitate the formation of two-dimensional structures.

DOI: 10.1103/PhysRevLett.94.145504 PACS numbers: 61.10.Eq, 66.10.Cb, 81.07.-b, 82.35.Np

Metal nanoparticles dispersed in polymeric matrices can self-assemble to form complex nanocomposites, such as a hierarchically self-assembled metal nanostructure on an ultrathin diblock copolymer scaffold [1], which is of great interest in the fabrication of novel electronic, magnetic, and photonic devices. Since the entire ordering process takes place far from equilibrium conditions, a controlled self-assembly of nanostructures in two dimensions (2D) has to be guided by a thorough understanding of ordering kinetics and nanoparticle dynamics in the composites. This requires measurement of their lateral diffusion transport in 2D and *in situ* and in real time with subnanometer spatial resolution. This has been difficult because of the paucity of the particles (often consisting of a submonolayer) and of the random particle distribution before they become ordered. To overcome these difficulties, for the first time, we have developed and used a novel method combining x-ray waveguide-based resonance-enhanced x-ray (REX) scattering [2] and grazing-incidence small-angle x-ray scattering (GISAXS) [3] to elucidate the real-time lateral distribution and diffusion of a Au nanoparticle submonolayer embedded in an ultrathin film polymer matrix.

In thin films, REXs can be achieved either in a low electron density layer (LEDL, e.g., polymer) deposited onto an x-ray mirror with high electron density [2] or in a LEDL sandwiched between a thin cap layer with high electron density and an x-ray mirror [4–7]. When the period of the x-ray standing waves, formed in the LEDL due to total external reflection upon the mirror, coincides with a submultiple of the thickness of the LEDL, a significant enhancement between 10 and 100 times of the electric field intensity (EFI) [2] can be observed and be used to increase the total x-ray scattering intensity proportionally, so that weakly scattering structures can be probed in a time-resolved manner.

The submonolayer of Au nanoparticles is synthesized by thermal evaporation and sandwiched between two layers of poly (*tert*-butyl acrylate) (PtBA) of equal thickness of ca. 35 nm deposited by spin coating [8,9]. The formation of Au nanoparticles follows Volmer-Weber growth mode attributed to the polymer-metal interaction being much weaker than that between the metal atoms [10]. PtBA (polydispersity index <1.2, glass transition temperature $T_g = 49\,^{\circ}\mathrm{C}$) used in the study has a molecular weight of 352 kg/mol corresponding to a radius of gyration (R_g) of 15 nm. The morphology of as-deposited Au nanoparticles in the polymer matrix is revealed by transmission electron microscopy (TEM) [Fig. 1(a)], where the diameter of the nanoparticles ranges from 2 to 4 nm and the average distance between the particles is ca. 6 nm. To generate REXs, the substrate to support the polymer-metal nanocomposite thin film was chosen to be a 50 nm-thick Ag mirror prepared by thermal evaporation on a flat float glass substrate with a 5 nm-thick Cr adhesive layer, shown

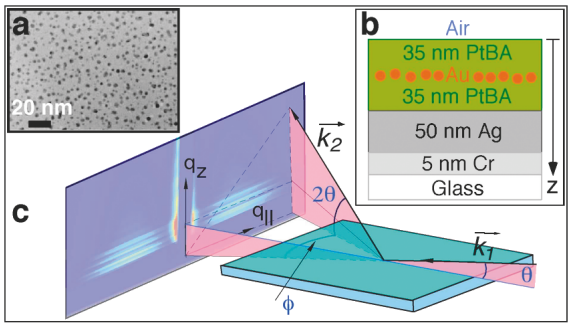

FIG. 1 (color). (a) TEM of as-deposited polymer-Au nanocomposite thin film, (b) schematic of the sample structure, (c) schematic of the GISAXS measurement configuration; the incident and scattered wave vectors are k_1 and k_2, θ is the grazing-incidence angle of the x-ray beam, ϕ and 2θ are the azimuthal and exit scattering angles, respectively, and $q_{\|}$ and q_z are the lateral and vertical components of the momentum transfer, respectively.

schematically in Fig. 1(b). Figure 1(c) shows the schematic of scattering geometry of GISAXS where the x-ray beam intercepts the sample at grazing incidence and the scattering pattern is recorded in 2D using an image plate detector. GISAXS and x-ray reflectivity (XRR) measurements were carried out at 1-BM and 8-ID beamlines at the Advanced Photon Source (APS) at 8 keV and 7.66 keV, respectively.

The sample was first characterized by XRR, as shown in Fig. 2(a). The curve between the critical angles of the PtBA film (θ_{c1}) and the Ag mirror (θ_{c2}) clearly shows three sharp reflection minima, at which resonance enhancement of the EFI in the polymer layer takes place, as shown in Fig. 2(b). The EFI distribution in Fig. 2(b), calculated from the fitting parameters from XRR measurements, is more complicated than those reported previously [2,4–7], which is due to the x-ray standing waves being perturbed by the embedded Au nanoparticles. It can be clearly seen in Fig. 2(b) that the EFI at the location of the nanoparticles that is of interest is greatly enhanced at the first resonance mode (TE0) at $\theta_{\mathrm{TE0}} = 0.186°$. The significance of such a resonance enhancement can be experimentally demonstrated by measuring GISAXS patterns at [Fig. 2(c)] and away [Fig. 2(d)] from θ_{TE0} at $\theta_1 = 0.225°$. The insets illustrate the corresponding calculated EFI distribution. Moreover, at the resonance, unwanted scattering signal from the interfaces is greatly reduced as the E-field nodes coincide with the interfaces as shown in the inset of Fig. 2(c), which further improves the sensitivity of using REXs to probe the nanoparticles. Therefore, the REXs effectively become a one-dimensional (1D) nanoprobe with a width of ca. 30 nm.

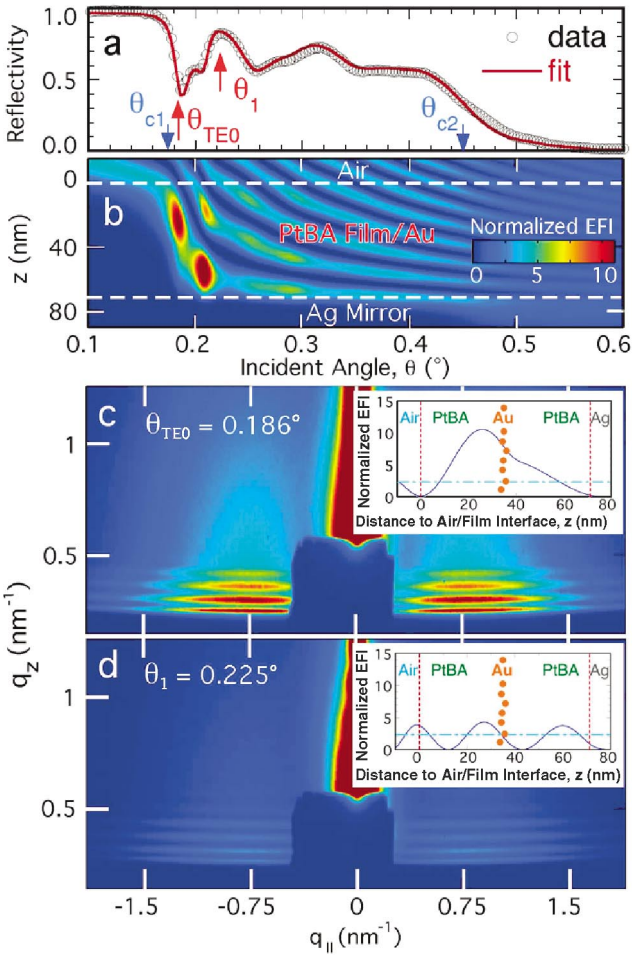

FIG. 2 (color). (a) Measured (open circles) and fitted (solid line) x-ray reflectivity curves of an as-deposited nanocomposite sandwich sample, (b) EFI plotted as a 2D map as a function of depth from the air-polymer interface ($z = 0$) and the incidence angle θ, (c) and (d) normalized 2D GISAXS measured at the first resonance condition (TE0 mode) and at off-resonance condition (θ_1), respectively. The insets depict the corresponding calculated E-field intensity distribution in the film. The strong specular reflections in (c) and (d) are blocked with a beam stop.

With the REX effect, not only does the GISAXS signal become greatly enhanced inside the film due to the enhanced EFI at the nanoparticle locations, but also the scattered x-rays exit the film only in certain discrete modes at a set of distinct angles. The values of these angles are equal to the incident angles at which REX occurs in the thin film demonstrating a perfect optical reciprocity [11]. At these exit angles, the measured scattering intensity is enhanced once more by the waveguiding interference (analogous to the incident x-ray enhancement) of the scattered photons between the two interfaces of the nanocomposite film. It should be mentioned here that at the nonresonance condition, the enhancement of the scattered x-rays is still present since they are not collimated. To illustrate the second enhancement effect, a more rigorous simulation of the scattering pattern based on the distorted wave Born approximation [12] was carried out. The scattering intensity as a function of the momentum transfer q is given in this method by

$$I(q) \propto (\Delta\rho)^2 S(q_\parallel) \sum_{m,n=0}^{3} \int_{\mathrm{film}} dz \phi_{\mathrm{Au}}(z) D_m(q_{mz}, z) D_n^*(q_{mz}, z) \times F(q_\parallel, q_{mz}(z)) F^*(q_\parallel, q_{nz}(z)), \quad (1)$$

where $D_0 = E_1^T E_2^T$, $D_1 = E_1^T E_2^R$, $D_2 = E_1^R E_2^T$, $D_3 = E_1^R E_2^R$, and $q_{0z} = k_{1z} + k_{2z}$, $q_{1z} = k_{1z} - k_{2z}$, $q_{2z} = -q_{1z}$, $q_{3z} = -q_{0z}$, respectively. $q_\parallel$ is the in-plane component of the momentum transfer $q = \sqrt{q_\parallel^2 + q_z^2}$, $\Delta\rho$ is the electron density contrast between the matrix and the particles, $S(q_\parallel)$ is the in-plane structure factor due to the lateral correlation of the nanoparticles, and $\phi_{\mathrm{Au}}(z)$ and $F(q)$ are the volume fraction and the form factor of the particles, respectively. The electric field amplitudes $E_{1,2}^T$ and $E_{1,2}^R$ of transmitted and reflected waves in the film are defined for incident wave vector k_1 and for scattered wave vector k_2, respectively, and account for the EFI redistribution in and out of the thin film which gives rise to the strong intensity fringes along the q_z direction. The form factor for spherical particles and the structure factor are given by [13]

$$F(q) = \frac{4}{3}\pi R^3 \left(\frac{\sin(qR) - qR\cos(qR)}{(qR)^3} \right), \quad (2)$$

$$S(q_\parallel) = \frac{1-\exp(-2q_\parallel^2\sigma_d^2)}{1-2\exp(-q_\parallel^2\sigma_d^2)\cos(q_\parallel d)+\exp(-2q_\parallel^2\sigma_d^2)}, \quad (3)$$

where R is the mean radius of the nanoparticles, and d is the average separation between the nanoparticles with a dispersion width σ_d. Figures 3(a) and 3(b) demonstrate an excellent agreement between the measured and simulated data [14]. One-dimensional cross-sectional scans of the 2D pattern along q_z and $q_\parallel$ directions with fits to the data are shown in Fig. 3(c) and its inset, respectively. While the q_z scan reveals the form factor of the nanoparticle perpendicular to the film interfaces convoluted with the enhanced and redistributed EFI effect, the $q_\parallel$ scan unambiguously determines both the lateral form factor and the structure factor of the nanoparticles [13]. The quality of the data and fits also demonstrate that, with the resonance enhancement, GISAXS is well suited for obtaining quantitative and statistical information on dilute nanoparticle morphology on a subsecond time scale, which makes it possible to elucidate the kinetics of the lateral motion of the nanoparticles. With the sample being the waveguide itself, no coupling [4–7] is needed to port the x-ray beam from the waveguide, which avoids any efficiency loss due to the coupling.

In order to probe the real-time diffusion of nanoparticles, the sample was heated *in situ* to the desired temperature and GISAXS data were collected as a function of time. The x-ray reflectivity data and their Fourier transforms indicate that, as soon as the sample was heated to 65 °C, the two layers became a single layer and the nanoparticles were embedded in the single polymer layer rather than between the two successively deposited layers (data not shown). The sample was moved transversely to the beam to expose a fresh spot of the sample after few exposures to avoid radiation damage. Upon annealing at 75 °C (well above PtBA T_g of 49 °C), the lateral motion of the nanoparticles in the polymer matrix became evident. Figs. 4(a)–4(c) show the real-time GISAXS patterns recorded at 0 min, 10 min, and 47 min after the sample temperature reached 75 °C. The scattering intensity distribution along the $q_\parallel$ direction recorded as a function of time is analyzed according to Eqs. (1)–(3), and the results are shown in Figs. 4(d)–4(f). The fits to the experimental data in $q_\parallel$ direction yield the quantitative values of d and σ_d at various instances during the annealing process. It can be readily observed that the intensity modulation along the $q_\parallel$ direction broadens as a function of annealing time. If the lateral or in-plane diffusion of nanoparticles were random as in Brownian motion, the in-plane correlation would remain invariant; hence no change would be observed in the GISAXS patterns over time. The broadening of the intensity distribution along $q_\parallel$ as a function of annealing time implies that the lateral diffusion of the Au nanoparticles in the PtBA matrix is dominated by other mecha-

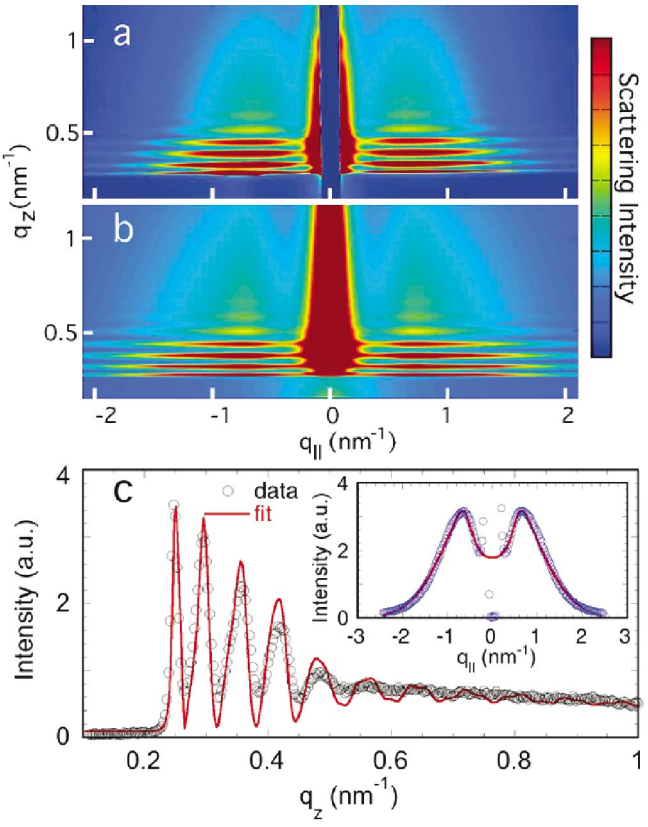

FIG. 3 (color). (a) and (b) Measured and simulated reciprocal space $q_\parallel - q_z$ GISAXS patterns of an as-deposited PtBA sandwich sample, respectively, (2 s exposure). The strong specular streak in (a) is blocked with a beam stop. (c) Measured (open circles) and fitted (line) intensity cross section drawn along the q_z direction from (a) and (b), with inset showing the measured (open circles) and fitted (line) intensity cross section along the $q_\parallel$ direction.

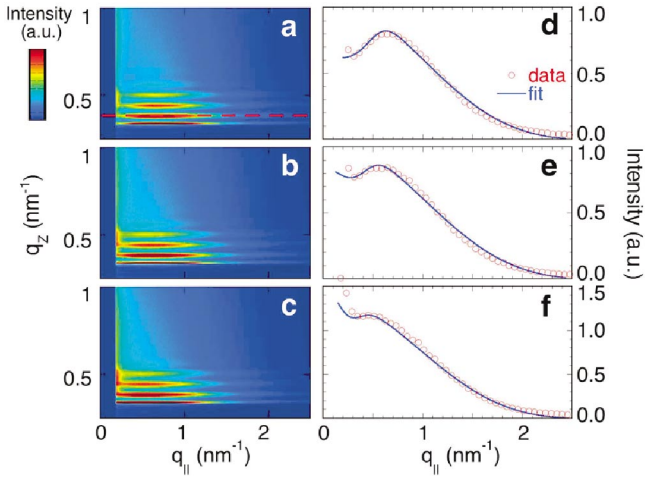

FIG. 4 (color). Measured reciprocal space $q_\parallel - q_z$ intensity map of GISAXS patterns recorded at a temperature of 75 °C at (a) 0 min, (b) 10 min, and (c) 47 min with (d), (e), and (f) the corresponding measured (open circles) and fitted (line) intensity cross section drawn along the $q_\parallel$ direction. The patterns were recorded at a time interval of 1 min with an exposure time of 2 s. The data were not sensitive to the polydispersity in the size of the nanoparticles due to small R and large σ_d.

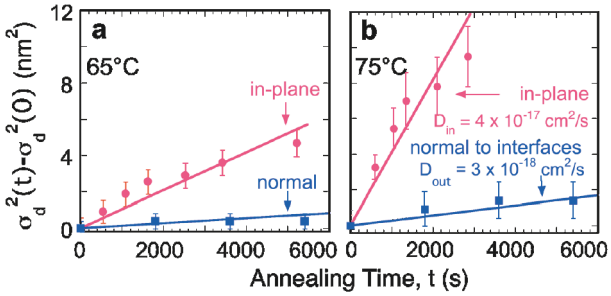

FIG. 5 (color). Lateral diffusion of the Au nanoparticles at temperatures (a) 65 °C and (b) 75 °C. For comparison, $\sigma_d^2(t) - \sigma_d^2(0)$ as a function of time normal to the film interfaces measured using an x-ray–standing-wave–based technique (Ref. [9]) is also shown.

nisms. The dominating driving force for the in-plane motion of nanoparticles is attributed to the attractive van der Waals interaction between the Au nanoparticles leading to their coalescence [10]. At short time scales, it can also be deduced from the analysis of the GISAXS patterns along the q_z direction (form factor) that the diffusion length is less than the average particle separation since the average size of the Au nanoparticles has not changed. In the initial stages of diffusion leading to coalescence, but well before the collision of the nanoparticles, d remains the same due to invariant particle number density. σ_d becomes larger as pairs of particles that are already close together move towards one another and pairs of particles that are already comparatively far apart move still farther apart. Thus, this manifests a constant d accompanied by an increase in σ_d. The resultant change in σ_d is a direct measure of the diffusion length of the nanoparticles. The lateral nanoparticle diffusion or the coalescence coefficient can be defined as $D = [\sigma_d^2(t) - \sigma_d^2(0)]/\Delta t$, where Δt is time interval [15], as shown in Figs. 5(a) and 5(b), at the temperatures 65 °C and 75 °C, respectively. For comparison, the values of $\sigma_d^2(t) - \sigma_d^2(0)$ of the Au nanoparticles in the out-of-plane direction measured in a separate experiment [9] are also shown. From a linear fit to the $\sigma_d^2(t) - \sigma_d^2(0)$ vs t relationship, the diffusion coefficient at 75 °C is determined to be 4×10^{-17} cm^2/s in the lateral direction as opposed to 3×10^{-18} cm^2/s in the direction normal to the thin film interfaces. These out-of-plane diffusion coefficients are considerably larger than those measured on large length and time scales. This can be explained when the nanoparticles move more freely as they are viewed as in a ''transient'' network with a mesh size (ca. 60 Å) smaller than the typical polymer molecular size [9]. The much faster lateral motion of the Au nanoparticles and their tendency to coalesce could be attributed to the following factors: (i) the correlation and the van der Waals attractive interaction between the Au nanoparticles exist only in the lateral direction as in a monolayer form, (ii) mobility of the polymer chains perpendicular to the interfaces is reduced due to the confinement in the films with thicknesses only several times larger than the R_g [16]. This mobility reduction is even stronger near the polymer-substrate interface [9].

In conclusion, we demonstrate that the lateral mobility of the nanoparticles is more than an order of magnitude higher than that normal to the interfaces at the measuring temperatures. In order to form laterally ordered 2D nanostructures, it is essential to have such a large disparity in the mobility. This study could thereby lead to a better understanding towards controlled nanostructure formation for microelectronic applications [17], as well as the unique diffusive properties of nanoparticles in a confined geometry defined by the ultrathin films. This x-ray nanoprobe resulting from resonance enhancement can also be extended to study the dynamics of the nanoparticles over shorter time scales (ms) during the initial diffusion through Brownian motion, by probing the time-correlated speckle patterns of coherent x-ray scattering [18] from the nanoparticles in ultrathin films. This will also throw light on various fundamental problems, such as elucidating glass transitions in polymer films [19]. Finally, this work has demonstrated the absolute necessity of analyzing GISAXS data using the dynamical scattering method outlined in this Letter.

The authors thank A. Gibaud and K. Shull for their participation and discussions, and S.-K. Cheong and the staff at 1-BM and 8-ID beamlines for assistance in the GISAXS measurements. This work and the use of the APS are supported by the U.S. DOE, BES, under Contract No. W-31-109-Eng-38. The work was also partially funded by NSF Grant No. DMR-0209542.

[1] W. A. Lopes and H. M. Jaeger, Nature (London) **414**, 735 (2001).
[2] J. Wang, M. J. Bedzyk, and M. Caffrey, Science **258**, 775 (1992).
[3] M. Rauscher *et al.*, Phys. Rev. B **52**, 16855 (1995).
[4] F. Pfeiffer *et al.*, Science **297**, 230 (2002).
[5] Y. P. Feng *et al.*, Phys. Rev. Lett. **71**, 537 (1993).
[6] S. Lagomarsino *et al.*, J. Appl. Phys. **79**, 4471 (1996).
[7] F. Pfeiffer, U. Mennicke, and T. Salditt, J. Appl. Crystallogr. **35**, 163 (2002).
[8] D. H. Cole *et al.*, Phys. Rev. Lett. **78**, 5006 (1997).
[9] R. S. Guico *et al.*, Macromolecules **37**, 8357 (2004).
[10] M. S. Kunz, K. R. Shull, and A. J. Kellock, J. Appl. Phys. **72**, 4458 (1992).
[11] M. Born and E. Wolf, *Principles of Optics* (Pergamon, New York, 1980).
[12] S. K. Sinha *et al.*, Phys. Rev. B **38**, 2297 (1988).
[13] G. Vignaud *et al.*, J. Phys. Condens. Matter **9**, L125 (1997).
[14] D. R. Lee *et al.* (to be published).
[15] P. Jensen, Rev. Mod. Phys. **71**, 1695 (1999).
[16] J. Wang *et al.*, Phys. Rev. Lett. **83**, 564 (1999).
[17] D. Y. Godovsky, Adv. Polym. Sci. **153**, 163 (2000).
[18] S. B. Dierker *et al.*, Phys. Rev. Lett. **75**, 449 (1995).
[19] R. Weber *et al.*, Phys. Rev. E **64**, 061508 (2001).